Pharmacological Research 204 (2024) 107207

Contents lists available at ScienceDirect

Pharmacological Research

journal homepage: www.elsevier.com/locate/yphrs

Decreased circulating IPA levels identify subjects with metabolic comorbidities: A multi-omics study

Marta Ballanti [a,b,1], Lorenzo Antonetti [b,1], Maria Mavilio [b], Viviana Casagrande [b], Alessandro Moscatelli [b,c], Daniele Pietrucci [d], Adelaide Teofani [e], Chiara Internò [b], Marina Cardellini [a,b], Omero Paoluzi [f], Giovanni Monteleone [b,f], Philippe Lefebvre [g], Bart Staels [g], Geltrude Mingrone [h,i,j], Rossella Menghini [b], Massimo Federici [a,b,*]

[a] Center for Atherosclerosis and Internal Medicine Unit, Policlinico Tor Vergata University Hospital, Via Oxford 81, Rome 00133, Italy
[b] Department of Systems Medicine, University of Rome Tor Vergata, Rome 00133, Italy
[c] Laboratory of Neuromotor Physiology, Santa Lucia Foundation IRCCS, Rome, 00179, Italy
[d] Department for Innovation in Biological, Agro-Food and Forest Systems (DIBAF), University of Tuscia, 01100 Viterbo, Italy
[e] Department of Biology, University of Rome Tor Vergata, 00133 Rome, Italy
[f] Unit of Gastroenterology, Policlinico Tor Vergata University Hospital, Via Oxford 81, 00133 Rome, Italy
[g] University of Lille, Inserm, CHU Lille, Institut Pasteur de Lille, U1011 EGID, Lille France
[h] Department of Internal Medicine, Catholic University, 00168 Rome, Italy
[i] Fondazione Policlinico Universitario A. Gemelli IRCCS, 00168 Rome, Italy
[j] Diabetes and Nutritional Sciences, Hodgkin Building, Guy's Campus, King's College London, London WC2R 2LS, UK

ARTICLE INFO

Keywords:
IPA
Gut
Cross-omics
Untargeted metabolomics
Genomics
Diagnostic
Data integration
Next-generation sequencing
Next-generation metabolic screening
Diabetes
Hyperglycaemia

ABSTRACT

In recent years several experimental observations demonstrated that the gut microbiome plays a role in regulating positively or negatively metabolic homeostasis. Indole-3-propionic acid (IPA), a Tryptophan catabolic product mainly produced by C. Sporogenes, has been recently shown to exert either favorable or unfavorable effects in the context of metabolic and cardiovascular diseases. We performed a study to delineate clinical and multiomics characteristics of human subjects characterized by low and high IPA levels. Subjects with low IPA blood levels showed insulin resistance, overweight, low-grade inflammation, and features of metabolic syndrome compared to those with high IPA. Metabolomics analysis revealed that IPA was negatively correlated with leucine, isoleucine, and valine metabolism. Transcriptomics analysis in colon tissue revealed the enrichment of several signaling, regulatory, and metabolic processes. Metagenomics revealed several OTU of *ruminococcus, alistipes, blautia, butyrivibrio and akkermansia* were significantly enriched in ^{high}IPA group while in ^{low}IPA group *Escherichia-Shigella*, *megasphera*, and *Desulfovibrio* genus were more abundant.

Next, we tested the hypothesis that treatment with IPA in a mouse model may recapitulate the observations of human subjects, at least in part. We found that a short treatment with IPA (4 days at 20/mg/kg) improved glucose tolerance and Akt phosphorylation in the skeletal muscle level, while regulating blood BCAA levels and gene expression in colon tissue, all consistent with results observed in human subjects stratified for IPA levels. Our results suggest that treatment with IPA may be considered a potential strategy to improve insulin resistance in subjects with dysbiosis.

1. Introduction

In recent years several experimental observations demonstrated that the gut microbiome plays a role in regulating positively or negatively metabolic homeostasis [1]. Large part of this effect is consequent to microbe imbalance or functional changes, resulting in the increased or diminished production of metabolites which exert signaling actions via known and unknown receptors [2]. Among gut-microbiota derived

Abbreviations: IPA, indolepropionate; HFD, High-fat diet; ^{high}IPA, High indolepropionate group; ^{low}IPA, low indolepropionate group.

* Correspondence to: Department of Systems Medicine, University of Rome Tor Vergata, Via Montpellier 1, Rome 00133, Italy.
E-mail address: federicm@uniroma2.it (M. Federici).

[1] Equally contributed

https://doi.org/10.1016/j.phrs.2024.107207
Received 13 March 2024; Received in revised form 5 May 2024; Accepted 5 May 2024
Available online 9 May 2024

metabolites those belonging to the three metabolic pathways of tryptophan (Trp), histidine (His), and phenylalanine (Phe) are known to affect various chronic inflammatory conditions, such as obesity, diabetes, arthritis, colitis, atherosclerosis, and neuroinflammation [3].

Indole-3-propionic acid, a Tryptophan catabolic product mainly produced by C. Sporogenes, has been recently shown to exert either favorable or unfavorable effects according to the experimental context and the model disease tested (4−22).

Regarding effects to protect from metabolic dysfunction there are several studies suggesting a role for indole derived tryptophan metabolites to protect from metabolic stress [4,5]. In metabolic compromised high-fat diet (HFD)-fed mice IPA reduced increased intestinal permeability observed upon dietary challenge and in obese subjects, IPA levels are reduced relative to lean counterparts, and these levels increase 3 months after Roux-en-Y Gastric Bypass (RYGB) [6]. IPA has been recently shown to attenuate metabolic dysfunction-associated steatotic liver disease by improving fat metabolism and inflammation [7], an effect potentially mediated by dietary intervention [8,9]. Similarly, it was shown that IPA levels in patients exhibiting a rapid renal function decline were significantly reduced compared to the control patients [10].

However, more recent data do not support that indole-3-propionic acid (IPA) mediates beneficial metabolic effects [11]. In the context of cardiovascular disease, dietary IPA supplementation has been suggested to dampen atherosclerotic plaque development in $ApoE^{-/-}$ mice. In murine- and human-derived macrophages, administration of IPA promoted cholesterol efflux from macrophages and protects from heart failure [12–14]. However, another experimental observation on cardiomyocytes found that IPA acutely might promote maximal mitochondrial respiration, while chronic exposure led to mitochondrial dysfunction also in endothelial cells and hepatocytes. Another study found that IPA increased blood pressure in rats [15,16]. Other experimental studies found that IPA might have a role to improve axonal regeneration after nerve injury [17]. Moreover, IPA has been found negatively associated to multimorbidity and incident T2DM in large epidemiological studies [18–22].

Given the potential clinical implications of these experimental observations which may underline a role of IPA as biomarker or therapeutic agent we performed a study to delineate the main clinical and omics characteristics of subjects characterized by low IPA levels. To explore the phenotype of subjects with low circulating IPA levels healthy subjects without major chronic diseases participating in a national screening for intestinal cancer were recruited and submitted to a protocol to analyze insulin resistance and related clinical variables. The protocol included analysis of serum metabolome, colon transcriptomics and 16S Metagenomics.

2. Methods

2.1. Human cohort

The FLOROMIDIA database was already described [23]. All subjects gave written informed consent, validated and approved by the ethical committee of Policlinico Tor Vergata University of Rome (Comitato Etico Indipendente, approval number 113.15). The human subject cohort comprised 37 subjects recruited at the Department of Medicine Policlinico Tor Vergata. Sample size was not determined by statistical methods, given the exploratory nature of the project. Colon transcriptomic analysis was performed with Affymetrix HUGENE 2.0 ST ARRAY FORMAT 100 (GEO Accession Number: GSE158237); SOD2 expression levels normalized with RMA method were used in this study.

The study conforms to recognized ethical standards as in the Declaration of Helsinki.

2.2. Metabolomics (human)

Metabolomics in human serum was performed as already described [23]. Briefly after blood draw and metabolites extraction with methanol, two aliquots were used for reverse phase (RP)/Ultra Performance Liquid Chromatography-tandem Mass spectrometry (UPLC-MS/MS) analysis in positive and negative electrospray ionization (ESI) mode. Full scan mass spectra (80–1000 *m/z*) and data dependent MS/MS scans with dynamic exclusion were recorded in turns. Raw data were extracted, peak-identified and QC processed using the hardware and software of Metabolon (Durham, NC, USA). For all following analyses, filtered and imputed metabolome data were $\log_2$ transformed.

2.3. 16S targeted metagenomic sequencing (human study)

Data generation: The stool of human subjects were collected and previously described [23]. DNA was extracted from the cecal content of human stool using the QIAamp DNAStoolMini (Qiagen, Venlo, Netherlands) and the bacterial 16S rDNA gene was sequenced (Vaiomer SAS, Labège, France) as described by Lluch et al. [24]. The V3–V4 hyper-variable regions of the 16S rDNA gene were amplified from the DNA extracts during a first PCR step using universal 16S primers. The joint pair length was set to encompass 476 base pairs amplicon and include specificity for the 16S rDNA gene of 95 % of the bacteria in the Ribosomal Database Project. For each sample, a sequencing library was generated by the addition of sequencing adapters and multiplexing indexes during a second PCR step as described previously [23–25]. The pool was denatured, diluted, and loaded onto the Illumina MiSeq cartridge according to the manufacturer's instructions using MiSeq Reagent Kit v3 (2 × 300 bp Paired-End Reads; Illumina, San Diego, CA, USA). Sequencing data were processed using the QIIME2 DADA2 plugin [26] with the denoise-paired option and standard parameters. Taxonomic classification was performed by a Naïve Bayes classifier (sklearn) [27], which was trained on the SILVA database release 138 [28]. OTU counts were then further processed and analyzed by R (Versione 4.3.1) and MicrobiomeAnalyst (Version 2.0) [29]. A total read count of 561578 was discovered in the study with average counts per sample of 22463.12 (min. to max.: 19164–28150). We identified a total number of 2159 OTU. After filtering (low count filter: minimum count $\geq$ 4 and mean abundance in at least 20 % of samples and low variance filter: 10 % removed based on inter-quantile range) 323 OTU remained in the study. The generated OTU table was imported and further processed in R using the phyloseq package [30].

2.4. Bioinformatics analyses

2.4.1. Metabolite cluster generation via WGCNA and pathway enrichment analysis

We used limma R package [31] with adjusted P-Value $\leq$ 0.05 to identify differentially abundant metabolites. As a method to reduce the dimensionality of the metabolomics data weighted correlation network analysis (WGCNA) was done using the R WGCNA package [32]. A soft-thresholding power of 5 was chosen based on the scale-free topology fit index-curve. Using this value the unsigned correlation network adjacency was calculated. The topological overlap matrix dissimilarity (TOM) of the adjacency matrix was then clustered using the 'Ward.D' method. The resulting tree was cut using a hybrid tree-cutting algorithm that was implemented in the cutreeDynamic function using a deepSplit of 4 and minModuleSize of 15. This resulted in 7 modules, with 34 unassigned compounds. The names of the clusters were chosen arbitrarily as colors. The eigenvalues in each sample of the resulting clusters were used for further analyses. Compounds that were clustered into a WGCNA cluster were subjected to pathway enrichment analysis. The pathway information for each compound was reported by Metabolon (Durham, NC, USA). A one-sided Fisher test was used to determine if a pathway was enriched within a cluster. P-values were then adjusted

using Benjamini-Hochberg method and a cut-off of P $\leq$ 0.05.

2.4.2. Differential expression analysis and gene cluster generation via WGCNA (human study)

After filtering (low abundance: relative abundance lower that 3 % percentile threshold and variance percentile rank lower than 12 %) 24302 probes remained in the study by a total of 28181. We used limma [31] with adjusted P-Value $\leq$ 0.05 and logFC > |0.25| cut-off to identify differentially expressed genes. Using biomaRt R package 14761 protein coding and lncRNA genes localized on chromosomes from 1 to 22 has been selected for further analysis. KEGG enrichment analysis of up and down regulated genes has been carried out by ClusterProfiler R package. As a method to reduce the dimensionality of the transcriptomic data WGCNA R package has been used. A soft-thresholding power of 7 was chosen based on the scale-free topology fit index-curve. Using this value the unsigned correlation network adjacency was calculated. The topological overlap matrix dissimilarity (TOM) of the adjacency matrix was then clustered using the 'average' method. The resulting tree was cut using a hybrid tree-cutting algorithm that was implemented in the cutreeDynamic function using a deepSplit of 3 and minModuleSize of 50. This resulted in 10 modules with no unassigned genes. The names of the clusters were chosen arbitrarily as colors. The eigenvalues in each sample of the resulting clusters were used for further analyses. For each module KEGG Enrichment Analysis has been performed by ClusterProfiler R package.

2.4.3. Differential analysis of OTU count (human study)

To analyze and visually explore the hierarchical structure of taxonomic differences between the groups, data were scaled by total sum scaling and heat tree analysis (metacoder R package) with non-parametric Wilcoxon Rank Sum test [33] has been performed In combination with DESeq2 test [34]. OTU counts were transformed for DESeq2 with the phyloseq_to_deseq2 function of the phyloseq package and normalized using the Variance Stabilization of the DESeq2 R package. Then a Wald test has been used to compare differences in OTUs between ^{low}IPA and ^{high}IPA groups [23,34].

In brief, a generalized linear model is fitted to give the log2 fold change using a negative binomial distribution with estimated sample-specific size factors and gene-specific dispersion parameters. The Wald test (nbiomWaldTest of DESeq2) was then used to test for significance of the log2 fold change.

2.4.4. Metagenome functions prediction (human study)

Based on 16S rRNA gene sequencing data, functional abundances of microbial communities were predicted by PICRUSt2 software (version 2.5.1) [35].

PICRUSt2 PWY outputs were analysed by LefSe [36] and DESeq2 R packages. For LEfSe pathway abundance row data had been used as input; parameters were left at their defaults: *alpha* for ANOVA and Wilcoxon tests at 0.05, threshold of the logarithmic LDA score at 2.0. For DESeq2 data were normalized by the variance stabilization of DESeq2 R package.

2.5. Experimental animals

6 weeks old C57BL/6 mice were fed a High Fat Diet (HFD) (60 % of calories from fat, code D12492; Research Diets, New Brunswick, NJ) for 8 weeks and then treated with IPA dissolved in sterile PBS (pH 7.4) (20 mg/Kg) or placebo (PBS) by oral gavage for 4 consecutive days after 3 h fast [37].

Metabolic testing procedures have been described previously [38]. Briefly, for glucose tolerance tests animals were fasted for 16 h and injected with 2 g/kg body weight of glucose into the peritoneal cavity. Blood glucose concentrations were determined by using an automated Onetouch Lifescan Glucometer (Milpitas, CA). Insulin levels in serum were measured using commercial kit (Mercodia, Uppsala, Sweden). Skeletal muscle, liver and white adipose tissue (WAT) were collected from randomly selected high fat diet fed mice. Studies were performed only in male mice. Animal studies were approved by the University of Tor Vergata Animal Care and Use Committee and Ministry of Health, license no. 24/2017-PR.

2.5.1. Energy balance

Indirect calorimetry was performed using LabMaster (TSE Systems, Bad Homburg, Germany). All mice were acclimatized for 24 h before measurements. O2 consumption (VO2) and CO2 production (VCO2) were measured in individual mice at 15 min intervals during a 24-h period. VO2 is expressed as milliliters of O2 consumed per kilogram of body weight per minute. Carbon dioxide consumption (VCO2) is expressed as milliliters of CO2 produced per kilogram of body weight per minute. Glucose oxidation (in g/min/kg$^{0.75}$ = [(4.545 3 VCO2) 2 (3.205 3 VO2)]/1000) was calculated [39].

2.5.2. Gene expression analysis

Total RNA was isolated from colon and muscle using TRIzol reagents (Invitrogen, Eugene, OR). A total of 2 mg total RNA was reverse transcribed into cDNA using the High Capacity cDNA Archive kit (Applied Biosystems, Foster City, CA). Quantitative real-time PCR was performed on individual samples using an ABI PRISM 7700 System and TaqMan reagents (Applied Biosystems). Each reaction was performed in triplicate using standard reaction conditions: 1 cycle at 50°C for 2 min, 1 cycle at 95°C for 10 min, and 40 cycles each at 95°C for 15 s and 60°C for 1 min. Calculations were performed via a comparative cycle threshold method normalized by 18S.

2.5.3. Western blots

Western blots were performed on total tissue homogenates prepared as previously described [40]. The following antibodies were used: anti–phospho-Ser473 Akt (anti-rabbit, 9271, lot 15) and total Ak (anti-rabbit 9272, lot 25)t, anti-phospho-Thr202/Tyr204 p42/44 MAPK (anti-rabbit 9101, lot 26) and total p42/44 MAPK (anti-rabbit 9102 lot 23), anti-phospho-Ser176/Ser180 Ikkα/β (anti-rabbit 2697, lot 21), anti–phosphoThr180/Tyr182 p38 (anti-rabbit 9211, lot 23) and total p38 (anti-rabbit 9212, lot 23) (all from Cell Signaling Technology, Danvers, MA) and total Ikkα/β (Santa Cruz, anti-rabbit SC-7607, lot j060).

2.6. Statistical analysis

Data were analyzed and visualized using R, MicrobiomeAnalyst and GraphPad Prism (V10). The statistical analysis was carried out using Student t Test, Mann-Whitney U Test, Two-tailed Fisher's Exact Test and Kruskal Wallis Test when appropriate. Data are presented as means ± standard error mean (S.E.M.). A Benjamini-Hochberg Adjusted P-value $\leq$ 0.05 was statistically significant.

2.6.1. Software used

- R version 4.3.1
- R packages:
  - Limma 3.56.2
  - ggplot2 3.4.4
  - biomaRt 2.56.1
  - Vegan 2.6.4
  - WGCNA 1.72
  - Phyloseq 1.44.0
  - Metacoder 3.6.0
  - LefSE1.1.2
- FastQC v0.12.1
- Python 3.10.9
- Qiime2–2023.2
- MetaboAnalyst 5.0
- PICRUSt 2.5.2

- GraphPad Prism 10.0
- ExpressAnalyst
- *MicrobiomeAnalyst 2.0*

3. Results

3.1. IPA is negatively correlated with insulin resistance and obesity

In a preliminary scope metabolomic analysis performed in a sample of 37 subjects with different degrees of BMI (Table 1) we observed that IPA negatively correlated with BMI and HOMA-IR ($p<0.0001$ and $p<0.06$, respectively). Given the recent links between IPA and cardiometabolic risk we used the same database to investigate the phenome of individuals carrying low or high levels of IPA in the blood.

3.2. Clinical characteristics of subjects stratified for IPA levels

Comparative analysis of clinical and biochemical variables between subjects in the low IPA tertile (^{low}IPA) (n =12) vs the high IPA tertile (^{high}IPA) (n = 13) revealed that ^{low}IPA subjects had significantly increased BMI, waist and hip circumference, diastolic blood pressure, glycated hemoglobin, fasting plasma glucose, HOMA-IR, TNF-α and plasma glucose concentrations at 90 post oral glucose load. Volcano Plot analysis identified 15 significantly lower and 5 significantly higher levels of metabolites in ^{high}IPA compared to ^{low}IPA. Among the lower metabolites in ^{high}IPA are 2-aminobutyrate, sphingosine 1-phosphate, leucine and phenylalanine, while among the higher are N-oleoyltaurine, 1-linolenoyl-GPC (18:3)* and 1-linoleoyl-GPE (18:2)* (Fig. 1A).

3.3. WGCNA metabolomic cluster generation and module functional enrichment

To learn more on specific metabolic pathways associated with IPA serum levels, we performed a weighted correlation network analysis (WGCNA) on the serum metabolome data. After removal of not annotated compounds, 306 chemically identified metabolites were clustered in 7 metabolite clusters (Fig. 1B). Module labels and colors have been chosen arbitrarily. Significant enriched pathways in the clusters were identified; only the turquoise cluster did not enrich metabolic pathways (Fig. 1B). Pearson correlations between eigenvalues of the metabolic clusters and IPA values revealed 2 modules associated with IPA (Benjamini-Hochberg-adjusted $P \leq 0.05$) (Fig. 1C). Blue (leucine, isoleucine and valine metabolism) cluster negatively correlated with IPA, while red (Lysolipid, Fatty Acid-Monohydroxy) cluster positively associated with

Table 1
Clinical charateristics of subjects as part of the FLOROMIDIA cohort. Unpaired two-tailed Mann–Whitney U test or two-sided Fisher's exact test has been used when appropriate. A P-value ≤ 0.05 was considered to be statistically significant. ^{low}IPA and ^{high}IPA groups are comprised respectively of 12 and 13 samples. BMI: body mass index; SBP: systolic blood pressure; DBP: diastolic blood pressure; CVD: hystory of cardiovascular disease; FPG: fasting plasma glucose; GDR: glucose disposal rate; US steatosis: ultrasonorographic steatosis; WBC: white blood cells; CCA-IMT: common carotid artery intima media thickness; CB-IMT: carotid bulb intima media thickness.

	^{low}IPA			^{high}IPA						
	n	mean	StDev	n	mean	StDev	n	mean	StdDv	U-stat	p-value
BMI (kg/m2)	25	33,64	9,44	12	41,03	7,88	13	26,82	4,17	144	0,01
Oggt90 (mg/dl)	22	165,95	58,68	9	210,56	63,71	13	135,08	26,18	108,5	0,02
Waist (cm)	24	102,71	15,64	11	114	10,55	13	93,15	12,57	122	0026
Hip (cm)	24	108,63	9,78	11	115,36	8,28	13	102,92	6,89	125,5	0,02
HBA1c (mmol/mol)	25	38,48	7,43	12	43,08	8,15	13	34,23	2,69	132	0,02
TNF-α (pg/ml)	25	7,17	2,34	12	8,53	2,58	13	5,91	1,03	133	0,02
DBP (mmHG)	25	78,4	7,71	12	82,92	4,31	13	74,23	7,81	127,5	0,02
FPG (mg/dl)	25	102,08	27,19	12	115,75	33,42	13	89,46	7,68	127,5	0,03
HOMA-IR	25	3,42	1,97	12	4,4075	1,97	13	2,52	1,48	126	0,04
Diabetes (%)	25	20.		12	41.6		13	0		0	0,06
Oggt120 (mg/dl)	23	150,57	63,41	10	187,8	75,13	13	121,92	29,74	102,5	0,07
Resistin (pg/ml)	25	9918,05	6018,65	12	13,330,82	6881,67	13	6767,81	2296,12	121	0,07
SBP(mmHG)	25	126	10,86	12	130,42	8,03	13	121,92	11,53	118,5	0,08
Oggt60 (mg/dl)	23	172,39	50,65	10	202,3	56,95	13	149,38	28,75	100,5	0,09
C-reactive protein (mg/L)	22	4,06	6,79	11	6,43	8,75	11	1,69	2,15	92,5	0,10
HDL-cholesterol (mg/dl)	25	58,2	18,63	12	51,67	19,13	13	64,23	15,93	40	0,11
GOT (U/L)	23	19,83	6,29	12	22,75	7	11	16,64	3,14	98,5	0,12
Uricemia (mg/dL)	23	5,42	1,84	11	6255	1,94	12	4,65	1,34	97	0,14
Insulin (U/ml)	25	13,38	6,23	12	15,629	5,08	13	11,30	6,47	112	0,15
IL-6 (pg/ml)	25	3,55	2,58	12	4,31	2,44	13	2,85	2,51	111	0,16
IL-1 β (pg/ml)	25	0,51	0,47	12	0,28	0,14	13	0,73	0,56	46	0,17
Apo A1 (mg/dl)	15	159,4	23,69	4	141,25	22,57	11	166	20,42	9,5	0,22
US Steatosis (%)	20	75		11	90,91		9	55,56		0125	0,23
Cortisol (μg/dl)	21	8,37	2,08	12	7,8	2,21	9	9,14	1,61	34	0,29
Total cholesterol(mg/dl)	25	196,48	35,78	12	185,83	35,04	13	206,31	33,58	53	0,3
Apo B (mg/dl)	14	90,51	19,57	4	83	18,67	10	93,51	19,12	11	0,4
Triglycerides (mg/dl)	25	116,64	64,56	12	137,17	79,78	13	97,69	37,31	98,5	0,4
Age (years)	25	57,52	8,56	12	55,5	9,12	13	59,38	7,55	59,5	0,5
Right CCA-IMT (cm)	16	0,09	0,03	3	0,1	0,01	13	0,09	0,03	27	0,5
Hypertension (%)	25	56		12	66,67		13	46,15		0,42	0,6
Left CB-IMT (cm)	16	0,12	0,02	3	0,12	0,02	13	0,13	0,02	15	0,77
GGT (UI/L)	22	30,32	11,15	12	31,42	10,02	10	29	12,24	69	0,77
eGFR (ml/min)	25	87,92	37,38	12	84,33	35,09	13	91,24	39,08	86	0,8
HOMA B	25	163,12	124,49	12	159,45	136,41	13	166,52	112,27	70	0,8
Serum Creatinine (mg/dL)	25	0,85	0,22	12	0,88	0,25	13	0,83	0,19	72	0,9
Oggt30 (mg/dl)	23	153,78	33,47	10	160,7	42,61	13	148,46	22,8	70,5	0,89
Left CCA-IMT(cm)	16	0,1	0,03	3	0,09	0,0047	13	0,10	0,04	22	0,9
Right CB-IMT (cm)	16	0,12	0,04	3	0,12	0,02	13	0,12	0,04	18,5	1
WBC (u/μl)	25	6169,61	1850,24	12	6106,69	2385,17	13	6227,69	1151,09	78	1000
GPT (U/L)	24	28,42	7,42	12	28,5	7,7	12	28,33	7,13	73	1000
sex (female %)	25	44		12	41,67		13	46,15		1,2	1000
CVD (%)	25	8		12	8,33		13	7,69		0,91	1000

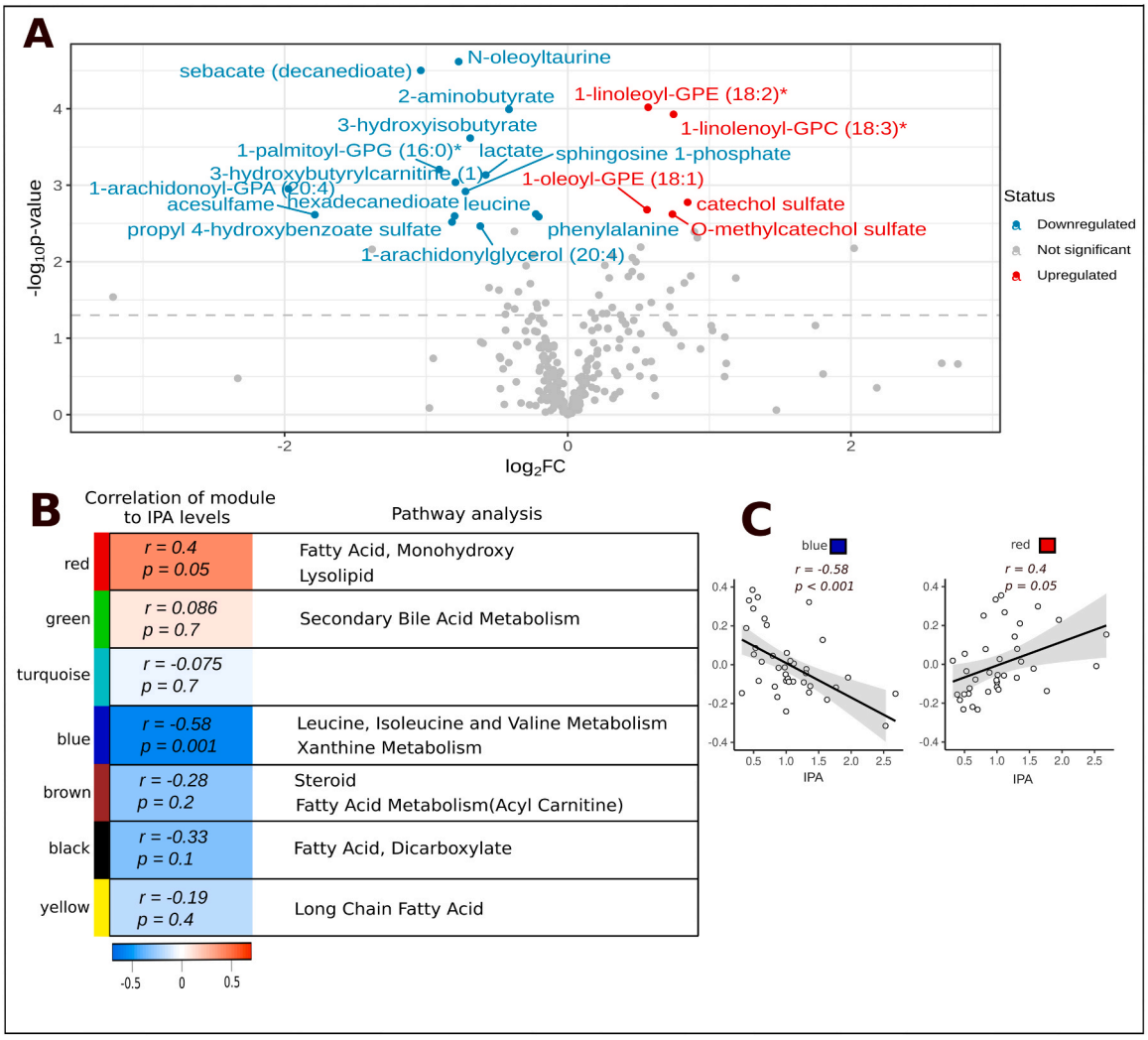

Fig. 1. (A) Volcano plot showing metabolites associated to IPA. No fold change cut off has been applied, only significant compounds are labeled. Two compounds (2-piperidinone (logFC −12, pvalue 0.035), 12-HETE (logFC −8, pvalue 0.086)) have been excluded from plot for better readability. (B) Clustering of serum metabolites by weighted correlation network analysis (WGCNA) resulting in 7 metabolites clusters (names and colors of the clusters were chosen arbitrarily). Eigenvalues of clusters were used for Pearson correlation analysis to IPA levels. Pearson correlation between WGCNA metabolite eigenvalues to IPA levels (P-values were adjusted using Benjamini-Hochberg method). Pathway enrichment analysis by one sided Fisher test (P-values Benjamini-Hochberg adjusted, a cut-off of $p \leq 0.05$ was chosen to determine if a pathway was significantly enriched). (C) Pearson correlation of eigenvalues of clusters to IPA levels revealed 2 metabolite clusters matching P-value cut off. All P-values were corrected for multiple testing using the Benjamini-Hochberg criterion.

IPA (Fig. 1C).

3.4. *WGCNA transcriptomics cluster generation and pathway enrichment analysis in colon*

To identify transcriptomic changes associated with IPA serum level variations in colon, transcriptomic comparative analysis between subjects in ^{low}IPA (n =12) and ^{high}IPA (n=13) has been performed by limma R package. Only protein coding genes and lncRNA from chromosome 1–22 were selected by the Biomart R package for further analysis, revealing respectively 889 and 189 up and down-regulated genes between the two groups with a log fold change cut-off of |0.25|. KEGG enrichment analysis of differentially expressed genes (Fig. 2A) by EnrichKegg R function revealed an enrichment of several signaling, regulatory and metabolic processes as insulin signaling pathway, longevity regulating mechanisms such as AMPK, RAS or MAPK signaling pathway and an involvement of genes in crucial biological processes as autophagy and adherens junctions (Fig. 1A).

To further identify gene expression changes associated with IPA level variations, weighted gene co-expression network analysis (WGCNA) in conjunction with functional enrichment analysis was performed. A total of 14761 protein-coding and lncRNA genes were clustered in 10 modules. Module labels and colors were arbitrarily chosen. Significant KEGG enriched pathways in the clusters were identified by *ClusterProfiler* R package. Pearson correlations between eigenvalues of the gene clusters and IPA values revealed 2 modules, turquoise and red (Fig. 2B,C), associated with IPA (Benjamini-Hochberg-adjusted $P \leq 0.05$). Turquoise module positively associated with IPA and KEGG enrichment analysis of genes clustered in this module confirmed a positive association between IPA and genes of insulin signaling pathway and tight junction. Red module, previously described as negatively associated with IPA, enriched non alcholic fatty liver disease, and diabetic cardiomyopathy; furthermore, those metabolic pathways exhibited a set of genes of COX and NDUF family shared with other biological processes such as oxidative phosphorylation, chemical carcinogenesis – reactive oxygen species, thermogenesis and neurodegenerative diseases like Alzheimer and Parkinson's disease. Gene Ontology enrichment analysis with cellular component ontology, confirmed an enrichment of genes involved in mitochondrial respiratory complex processes in the red cluster.

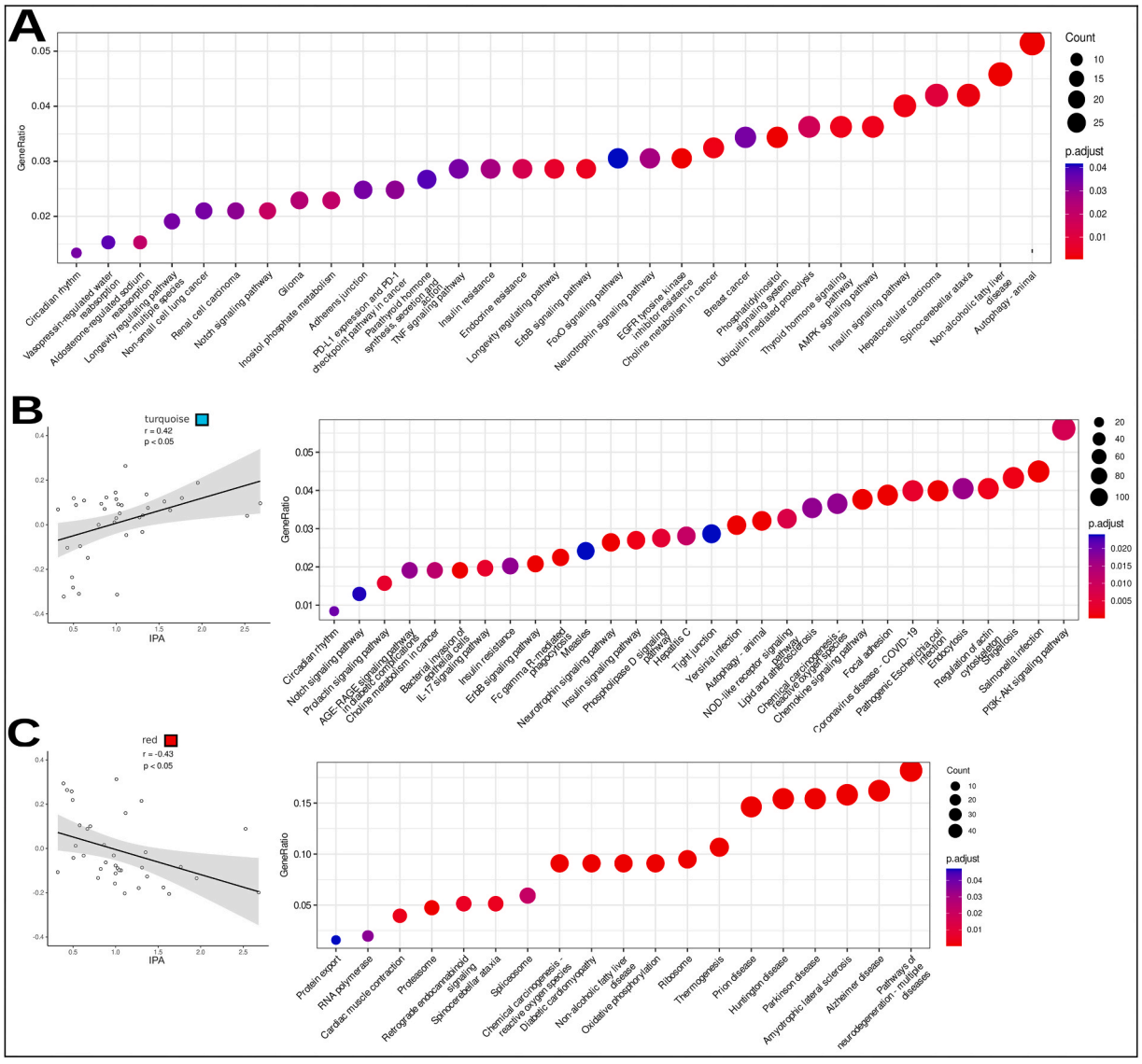

Fig. 2. (A) KEGG enrichment analysis of differentially expressed gene between ^{high}IPA and ^{low}IPA group (logFC cut-off |0.25|, p-values Benjamini-Hochberg adjusted). (B,C) Pearson correlation and KEGG enrichment analysis of WGCNA clusters significantly associated with IPA; the size of the dots in the dotplots represents the number of differentially expressed genes; the colour represents the significance of the enrichment.

3.5. 16S targeted metagenomic sequencing

To examine gut flora differences between subjects in low IPA tertile (^{low}IPA) (n =12) and high IPA tertile (^{high}IPA) (n = 13), 16S ribosomal rRNA targeted metagenomic sequencing of cecal content was performed (Fig. 3). Heat-tree analysis by metacoder R package revealed an increase in members of class Clostridia in ^{high}IPA caused by an expansion respectively of *Clostridiacea* family and *Clostridium_sensu_stricto_1* genus (Fig. 3B).

Consulting Arb-Silva browser we observed that this genus contains entries of *Clostridium perfringens, Clostridium Paraputrificum* and *Clostridium botulinum.* Relative abundance of cecal bacteria at class level confirmed an increase in class Clostridia members in ^{high}IPA group (Fig. 3A). To obtain a picture of gut bacterial diversity, we estimated *alpha* diversity by different indices, which revealed loss of diversity at genus level in ^{low}IPA group (Fig. 3C). A generalized loss of microbial quantity and microbial diversity in ^{low}IPA groups is observable also in heat-tree as well as a numerical, non-significative reduction in abundance of order *Lachnospirales* caused by a loss of *Lachnospira*, *Lachnospiraceae_ND3007_group* and *[Eubacterium]_xylanophilium_group* genera in the ^{low}IPA group.

3.6. Differential analysis of OTU count

Comparative analysis between the low and high IPA groups was performed by DESeq2. Results revealed several OTU belongings to Firmicutes phylum increased in ^{high}IPA group similarly to the heat tree analysis as well as the positive increase in clostridium_sensu_stricto_1 OTU (Fig. 4A). Furthermore several OTU of *ruminococcus*, *alistipes*, *blautia*, *butyrivibrio* and *akkermansia* were significantly enriched in ^{high}IPA group while in ^{low}IPA group *Escherichia-Shigella*, *megasphera* and *Desulfovibrio* genus were more abundant (Fig. 4A). *Roseburia* showed both increased and decreased OTUs in ^{high}IPA (Fig. 4A). However, when considering the top 20 most abundant genera *Roseburia* was altogether more abundant in ^{high}IPA group (Fig. 4B). Interestingly several *bacteroides* and *ruminococcus* OTU were more abundant in ^{high}IPA group while *prevotella* and *prevotella_9* enriched in ^{low}IPA.

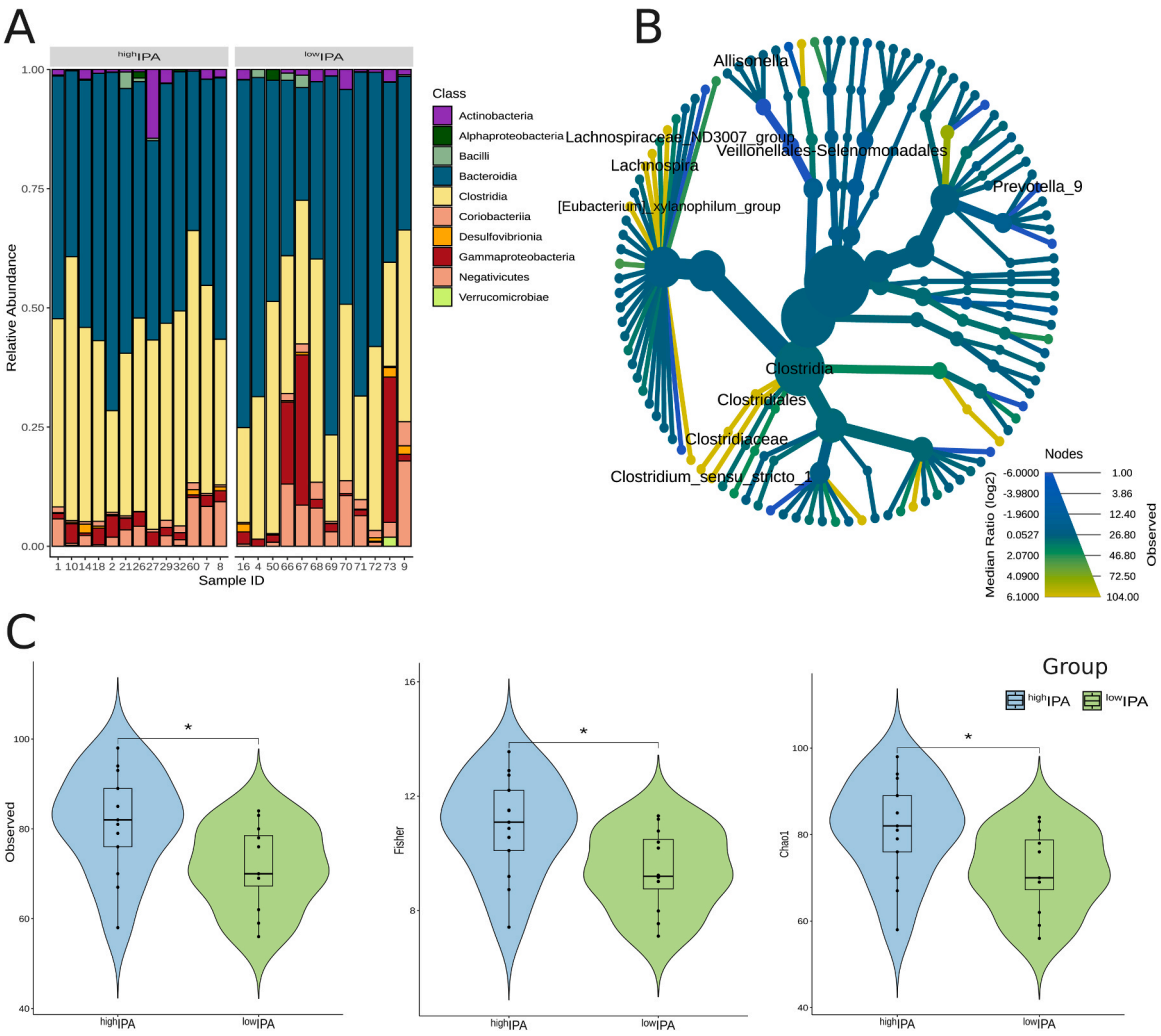

Fig. 3. (A) Relative abundance of cecal bacteria at Class level. (B) Analysis of gut microbiota differences between patients with low and high IPA serum levels. Heat-tree showing differences between microbial structure and composition. Size and color of nodes and edges are correlated with the abundance of organisms in each taxonomic category. Significant taxon names are labeled (Wilcoxon Rank Sum test P-value ≤ 0.05); (C) Alpha diversity of cecal microbiome by Observed, Fisher and Chao1 index (Unfiltered data has been rarefied to minimum sample sum for alpha-diversity analysis) at genus level.

3.7. Multiomics analysis

To identify specific gut microbiome changes associated with WGCNA serum metabolome clusters, we searched by DESeq2 OTUs associated with module eigenvalues of blue and red module. Module eigenvalues tertiles of each cluster has been used to identify the groups for differential abundance analysis (Fig. 4A). Only taxa with a Benjamini-Hochberg adjusted p-value <= 0.05 between IPA tertiles had been selected for the plot. As expected, taxonomic profile of samples with high values of red module eigenvalues was similar with that of high IPA serum levels group in opposition to samples with high blue module eigenvalues. Interestingly, several *prevotella_9* and *prevotella* were significantly associated with variations of eigenvalues of both red and blue WGCNA clusters. All *alistipes* OTU and several *bacteroides* that were previously shown enriched in ^{high}IPA group resulted significantly associated with serum meabolome WGCNA cluster eigenvalues variation. Both *lactobacillus* and *desulfovibrio* were positively and negatively associated respectively with blu and red WGCNA module, while we observed a non-significative increase of escherichia-shighella in samples with high blu WGCNA module eigenvalues and a significant negative association with both lysolipid WGCNA cluster and ^{high}IPA group; also, sutterella was significantly associated with red WGCNA module. Both *lactobacillus* and *butyrivbrio* showed a significant association with BCAA enriched WGCNA cluster, positive and negative respectively.

3.8. Metagenome functions prediction

To predict the microbial community functional profiles, the samples were processed by using PICRUSt2 software and the PWY outputs were analysed by LEfSe (Fig. 4C) and DESeq2 (Fig. 4D) to evaluate differences among ^{high}IPA and ^{low}IPA groups. Both softwares revealed an increased gene copy number related to enterobacterial common antigen biosynthesis in ^{low}IPA group. Furthermore, DESeq identified the super pathway of LPS biosynthesis as the pathway with the lower log2FC in ^{high}IPA samples (Fig. 4D) while LEfSe identified this pathway as marker of ^{low}IPA group with a pvalue ≤ 0.07. Controversely, only LEfSe found the chimeric pathway of O-antigen biosynthesis as marker of ^{high}IPA group.

3.9. Effects of IPA in mice undergoing diet-induced obesity for 12 weeks

To test the hypothesis that IPA directly affects, at least in part, the processes observed in human subjects, we fed WT mice a HFD for 8 weeks to induce an obese and insulin-resistant phenotype (Diet-Induced Obesity (DIO) mice). After 8 weeks, mice were subjected to a short-term treatment (4 days) with IPA (20 mg/kg) or PBS delivered by oral gavage (Fig. 5A). In this model we found that IPA slightly improved fasting

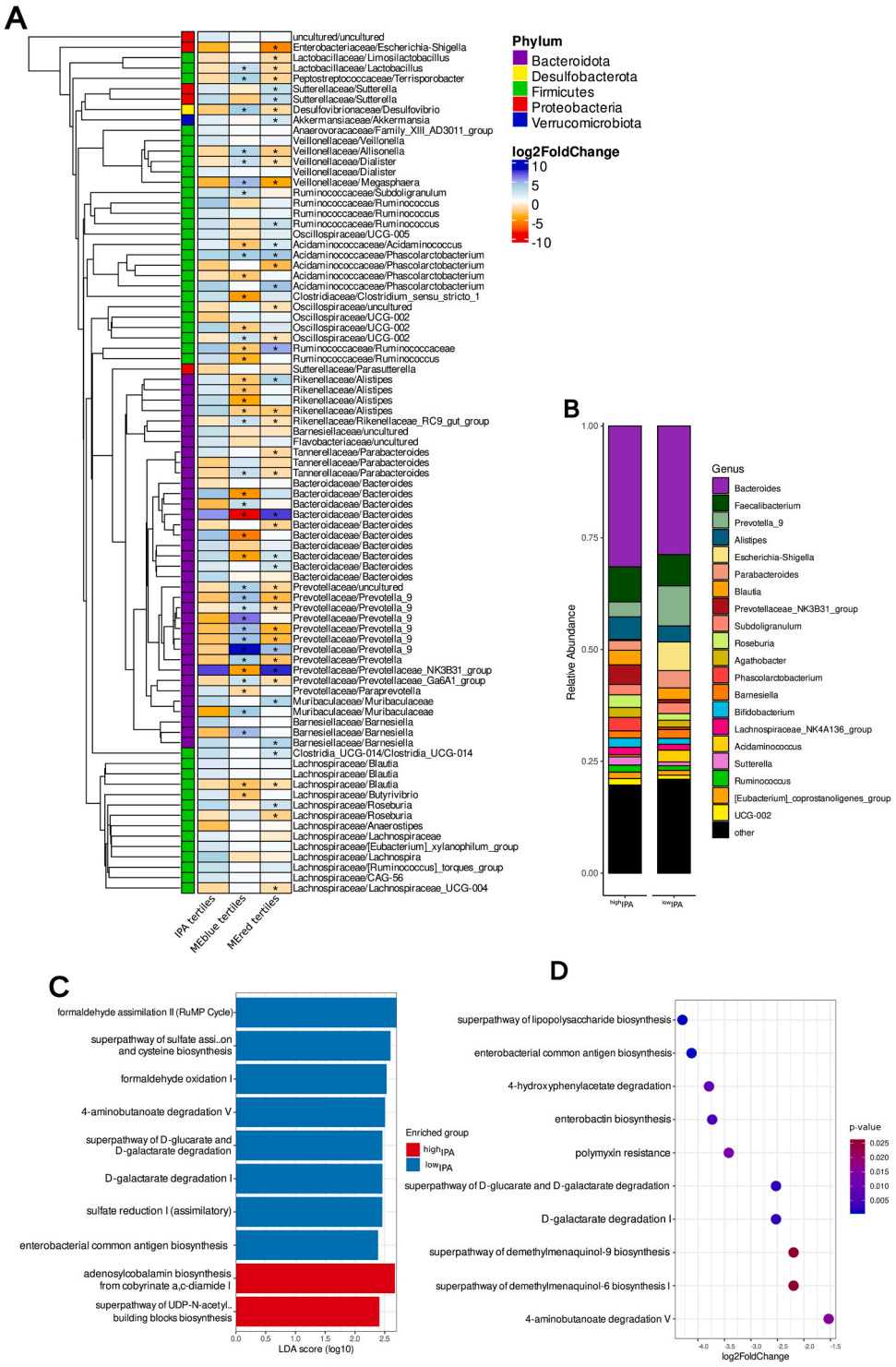

Fig. 4. (A) Taxa differentially abundant by DESeq2 between patients with low and high IPA serum levels and their associations with red and blue WGCNA serum metabolome clusters. Rows correspond to all significant taxa (Benjamini-Hochberg adjusted pvalue ≤ 0.05) between low and high IPA groups clustered by phylogenetic distance; for all taxa is reported the Family and Genus taxonomic rank. Blue and red denote positive and negative log2FC, respectively. The intensity of the colors represent the log2FC of the taxa between the samples stratified by tertiles of IPA serum leveles and eigenvalues of red and blue WGCNA serum metabolome clusters. Log2FC direction: second tertile (66.67th percentile) / first tertile (33.33rd percentile). Bacterial phyla are summarized by the color code on the first column. The dots indicate the associations that are significant (Benjamini-Hochberg adjusted pvalue ≤ 0.05). (B) Relative abundance of cecal bacteria at Genus level in ^{high}IPA and ^{low}IPA groups. (C) Linear discriminant analysis between ^{high}IPA and ^{low}IPA groups. LEfSe parameters were left at their default: Wilcoxon tests at 0.05, threshold of the logarithmic LDA score at 2.0. (D) DESeq2 Wald test to compare metagenomic prediction results between the two groups (P-values were adjusted using Benjamini-Hochberg method and a cut-off of $p \leq 0.05$ was chosen to determine if a pathway was significantly enriched).

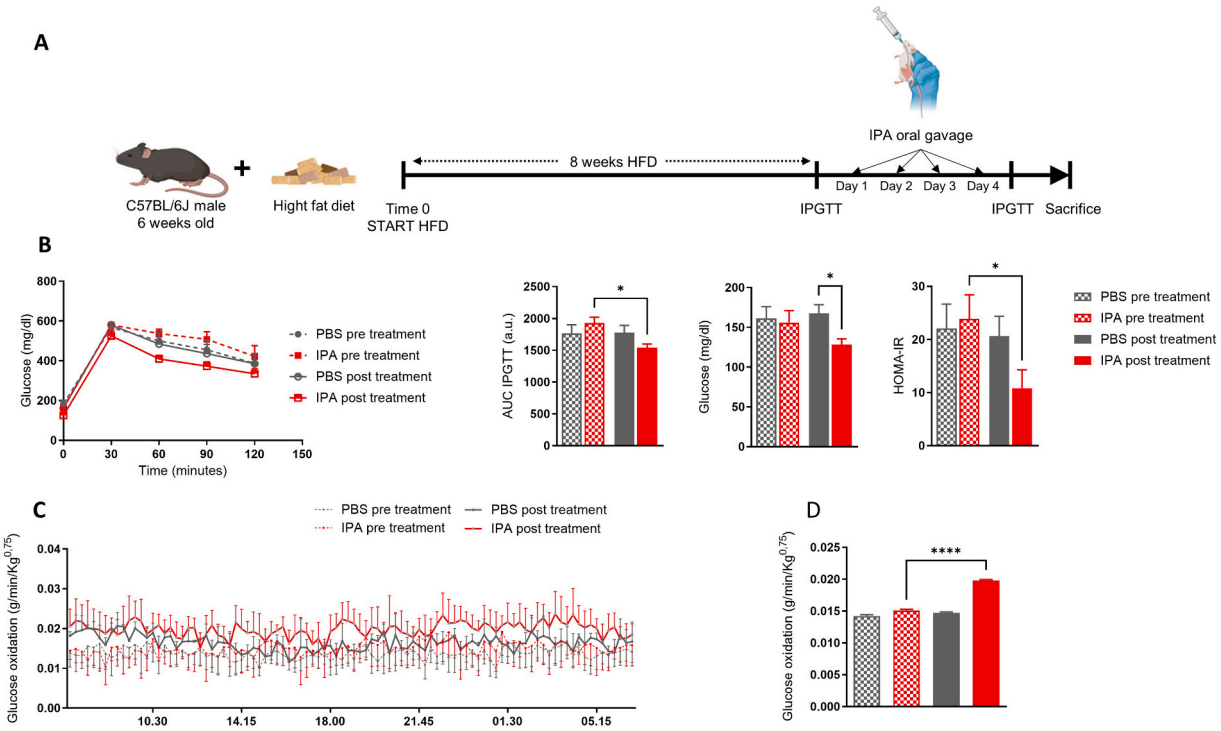

Fig. 5. Short time course of metabolic effects in DIO mice injected with IPA for four days. (A) Mice were treated with a HFD for 12 weeks and with IPA or PBS for 4 days in WT mice. (B) intraperitoneal glucose tolerance test (IPGTT), IPGTT areas under the curve (AUC), fasting glucose levels and insulin resistance (determinate by HOMA-IR), analyzed in serum obtained from HFD mice pre and post IPA treatment. (C, D) Amount of glucose oxidized calculated as described in Methods section. (**p≤0.05,****p≤0.0001; One-way Anova, data are means±SEM).

glucose and glucose tolerance in a glucose tolerance test (Fig. 5B). When subjected to indirect calorimetry we found that IPA significantly increased glucose oxidation (Fig. 5CandD).

Next, given the correlation of low grade inflammation with BCAA metabolism that emerged from colon transcriptomics and serum metabolomics analysis in human subjects, we analyzed signaling pathways and gene expression levels in colon tissue from DIO mice after IPA treatment. We found that IPA significantly decreased phosphorylation of *p38*, *Ikkα/β* and *Erk1/2* (p≤0.05) (Fig. 6A, B) in DIO mice. Genes involved in membrane permeability and dysbiosis such as *Zo-1*, *Claudin-*

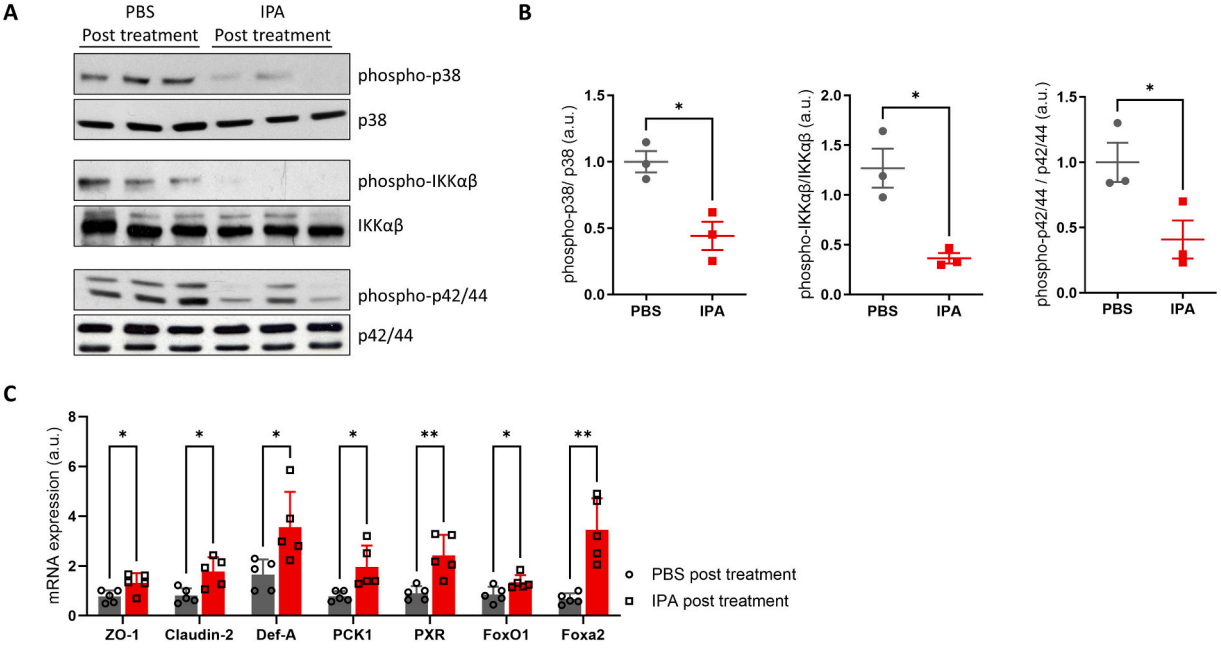

Fig. 6. Analysis of signaling pathways and gene expression in colon from DIO mice treated with IPA. (A) Protein levels and (B) quantification determined by densitometry of phospho p38 and total p38, phospho Ikkα/β and total Ikkα/β, phospho p42/44 MAPK and total p42/44 MAPK, in colon of PBS treated (n=3) and IPA treated (n=3) mice. (C) Zo-1, Claudin-2, Def-a, Pck1, Pxr, FoxO1 e Foxa2 gene expression in colon of PBS treated (n=5) and IPA treated (n=5) mice. (mRNA expression was determined by real-timePCR and normalized to b-actin mRNA) (*p<0.05, **p≤0.01; Student's t test, data are means±SEM). a.u.,arbitrary unit.

2 and *Def-a* were significantly increased in IPA treated DIO mice ($p \leq 0.05$). Moreover, in IPA treated mice we found increased expression of *Pck1*, *Pxr* ($p \leq 0.05$, $p \leq 0.01$) and genes involved in metabolic control, such as *FoxO1* and *Foxa2* ($p \leq 0.05$, $p \leq 0.01$).

Afterwards, given the effect observed on glucose oxidation we focused on skeletal muscle. We found that IPA treatment significantly improved *Akt* phosphorylation in randomly selected DIO mice treated with IPA (Fig. 7A, B). We noted that BCAA levels were significantly decreased in skeletal muscle from DIO mice treated with IPA compared to DIO mice treated with PBS ($p<0.05$) (Fig. 7C). We found that expression of BCAA degrading enzymes, such as *Bckdhb* and *Aldh6a1,* was significantly increased in muscle from DIO mice treated with IPA compared to DIO mice treated with PBS ($p<0.01$) (Fig. 7D).

Finally, IPA treatment in DIO mice did not significantly modulate hepatic and adipose Akt phosphorylation and neither tissue histology nor gene expression (Supplementary Figures 1 and 2).

4. Discussion

In this manuscript we compared the phenome of subjects with low and high circulating levels of 3-indole propionic acid (IPA), since this microbial derived compound was recently described as a potential bridge between intestinal dysbiosis and low-grade inflammation with repercussions on regulation of metabolic processes in the host. Subjects characterized by ^{low}IPA carry several features of metabolic syndrome and inflammatory and oxidative stress burden which are generally also associated to increased BMI, suggesting an intimate link between increased adiposity and the production of this metabolite from the intestinal microbiome.

Metabolomics confirmed this association since ^{low}IPA carry higher levels of metabolites linked to insulin resistance and oxidative stress such as sphingosine 1-phosphate, leucine, phenylalanine, 2-aminobutyrate. Sphingosine 1-phosphate may play a positive role on HDL metabolism and microangiopathy [41,42], although the roles of S1P are more controversial, because there are five cell-surface S1P receptors (S1PRs: S1P1-5R) which have altered functions, different cellular expression patterns, and inapparent intracellular targets. Recent findings, support the concept that the pharmacological activation of S1P1 or S1P3 improves obesity and associated metabolic disorders, whereas that of S1P2 has the opposite effect [43]. BCAA metabolism is a known risk factor for insulin resistance and Type 2 diabetes and increased Leucine as well as Isoleucine and Valine are known predictors for both Type 2 diabetes and CVD [44–46]. Restriction of Isoleucine and Valine in the diet has been shown to improve metabolic health [47]. Leucine has been shown to increase mitochondrial metabolism and lipid content without affecting insulin signaling in myotubes although increased Leucine level may reflect either its enrichment in the diet or defective catabolism while its deprivation is known to improve insulin sensitivity [48].

IPA is a tryptophan (Trp) metabolite produced by intestinal bacteria and influenced by the diet. Recent data suggest that C. Sporogenes possesses a reductive pathway able to modulate IPA levels in gnotobiotic mice [49]. Subjects carrying low IPA levels show signs of reduced microbiome alpha diversity. Reduced microbiome diversity is a hallmark of insulin resistance states including obesity, type 2 diabetes, NAFLD and cardiovascular diseases [50–52].

Large intestine is known to host gut microbes and enteroendocrine cells implicated in secretion of GLP1 and other hormones [53]. Thus, it may be speculated that these findings are explained by removal of GLP-1 producing cells which are enriched in the distal part of large intestine. However, the correlation of IPA with enteric hormones was mild. Therefore, it is conceivable that the effect may be mediated by alteration of colonic microbiota composition and the interaction with intestine function. The metabolic burden of large intestine remains unclear although a recent analysis provided support to effects on the development of Type 2 Diabetes, which is increased after colectomy compared other type of surgeries [54]. A link between diabetes and colonic

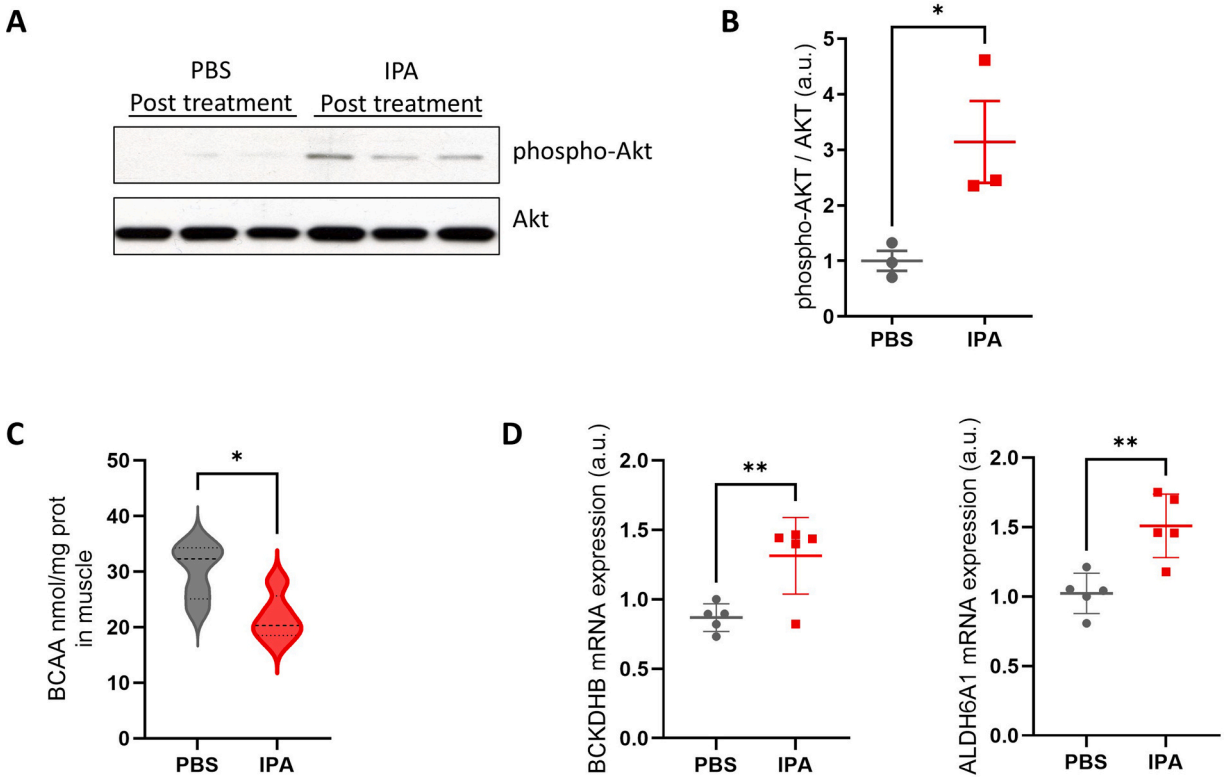

Fig. 7. Effects of IPA on BCAA degrading enzymes. (A) Protein levels and (B) quantification determined by densitometry of phospho Akt and total Akt, in muscle of PBS-treated (n=3) and IPA-treated (n=3) mice. (C) Intra-muscle BCAAs level and D) Bckdhb and Aldh6a1 gene expression in muscle of PBS-treated (n=5) and IPA-treated (n=5) mice. (mRNA expression was determined by real-time PCR and normalized to b-actin mRNA). a.u., arbitrary unit.

functions is also known in subjects with Type 1 Diabetes who suffer of high frequency of gastrointestinal (GI) disorders, named diabetic enteropathy, which is still poorly defined but involves regulation of intestinal stem cells [55,56].

Our enrichment analysis based on differential gene expression comparing subject with high and low IPA levels identified numerous KEGG pathways related to metabolic homeostasis including autophagy, Non Alcoholic Fatty liver disease, AMPK signaling pathway, Phospatidylinositol signaling system, FoxO signaling pathway. Similar results were obtained using WGCNA clusters which also highlighted the link among IPA and pathways related to the control of infection and inflammatory signal such as Chemokine signaling, NOD-like receptor signaling but also metabolic pathways. These results may also be determined by antioxidant and immune modulating effects of IPA which are similar to melatonin, another Tryptophan derived metabolite that regulates immunological status in subjects with cardiometabolic risk [57,58]. However, the capacity of IPA to scavenge hydroxyl radicals exceeded that of melatonin, an indoleamine considered to be the most potent naturally occurring scavenger of free radicals [59].

Our data suggest a link between IPA levels and metabolic alterations associated to insulin resistance and metabolic syndrome. IPA may exert its effects via modulation of inflammatory and metabolic transcriptional factors, such as NF-κB, PXR as well as mitochondrial function [37,60,61]. To test the hypothesis that IPA may directly exert metabolic functions we performed a very short term study exposing mice with diet induced insulin resistance to IPA or PBS as control. Our data support previous fidings in human or experimental settings since we observed that after IPA treatment mice showed a slight significant improvement in glucose tolerance, in part underlined by increased glucose oxidation. At colon level IPA reduced activation of signalling intermediates linked to stress and inflammation such as *p38*, *Ikkα/β* and *Erk* as well as determined increase in factors such as *Pck1*, *Pxr*, *FoxO1*, *Zo-1* and *Claudin-2* that altogether support favourable anti-inflammatory effects and improved gut barrier impermeability [62,63]. The effect on glucose oxidation evokes the possibility that IPA may regulate metabolic homeostasis at muscle level where we observed improved *Akt* activation after IPA treatment.

Our work has limitations, in fact the measurement of IPA has been performed only in the blood although since IPA is produced by intestinal microbiome it is conceivable that its effects reflect the synthesis in the intestinal lumen and the following absorption from the intestinal wall. Another limitation is the low number of subjects. Nevertheless, though a combination of in vivo and omics methods and confirmation with a physiology model our data support the potential role of IPA as an agent useful to improve metabolic homeostasis or as a biomarker in human subjects.

Funding

This work has been supported primarily by the MUR-PNRR (M4C2I1.3 PE6 project PE00000019 Heal Italia CUP: E83C22004670001) (to M.F.). This study was also funded in part by the Ministry of University and Research (MUR) Progetti di Ricerca di Interesse Nazionale (PRIN) [2017FM74HK], EFSD Sanofi Programme 2022, PON BIO-D ARS01_00876 (all to M.F.).

CRediT authorship contribution statement

Giovanni Monteleone: Writing – original draft, Methodology, Investigation. **Philippe Lefebvre:** Investigation, Data curation. **Marta Ballanti:** Investigation, Data curation. **Bart Staels:** Supervision, Investigation. **Lorenzo Antonetti:** Writing – original draft, Investigation, Data curation. **Geltrude Mingrone:** Validation, Resources, Methodology, Investigation. **Maria Mavilio:** Investigation. **Rossella Menghini:** Writing – review & editing, Writing – original draft, Project administration, Methodology, Investigation, Conceptualization. **Viviana Casagrande:** Supervision, Project administration, Methodology, Investigation. **Massimo Federici:** Writing – review & editing, Writing – original draft, Supervision, Funding acquisition, Conceptualization. **Alessandro Moscatelli:** Methodology, Investigation, Data curation. **Daniele Pietrucci:** Investigation. **Adelaide Teofani:** Investigation, Data curation. **Chiara Internò:** Methodology, Investigation. **Marina Cardellini:** Supervision, Project administration, Methodology, Investigation. **Omero Paoluzi:** Resources, Methodology, Investigation.

Declaration of Competing Interest

The authors declare not to have conflicts of interest concerning the content of this manuscript.

Data Availability

Data will be made available on request.

Acknowledgments

the authors confirm that they have full access to all data and bear the ultimate responsibility for the decision to submit them for publication. Graphical abstract figure created with BioRender.com

Appendix A. Supporting information

Supplementary data associated with this article can be found in the online version at doi:10.1016/j.phrs.2024.107207.

References

[1] A. Agus, K. Clément, H. Sokol, Gut microbiota-derived metabolites as central regulators in metabolic disorders, Gut 70 (2021) 1174–1182, https://doi.org/10.1136/gutjnl-2020-323071.
[2] J. Liu, Y. Tan, H. Cheng, D. Zhang, W. Feng, C. Peng, Functions of gut microbiota metabolites, current status and future perspectives, Aging Dis. 13 (2022) 1106–1126, https://doi.org/10.14336/AD.2022.0104.
[3] Xu H., Pan L.B., Yu H., Han P., Fu J., Zhang Z.W., et al., 2022. Gut microbiota-derived metabolites in inflammatory diseases based on targeted metabolomics. Front Pharmacol. 13, 919181. Gut microbiota-derived metabolites in inflammatory diseases based on targeted metabolomics.
[4] C. Teunis, M. Nieuwdorp, N. Hanssen, Interactions between tryptophan metabolism, the gut microbiome and the immune system as potential drivers of non-alcoholic fatty liver disease (NAFLD) and metabolic diseases, Metabolites 12 (2022) 514, https://doi.org/10.3390/metabo12060514.
[5] Y. Hu, J. Li, B. Wang, L. Zhu, Y. Li, K.L. Ivey, et al., Interplay between diet, circulating indolepropionate concentrations and cardiometabolic health in US populations, Gut 72 (2023) 2260–2271, https://doi.org/10.1136/gutjnl-2023-330410.
[6] M. Jennis, C.R. Cavanaugh, G.C. Leo, J.R. Mabus, J. Lenhard, P.J. Hornby, Microbiota-derived tryptophan indoles increase after gastric bypass surgery and reduce intestinal permeability in vitro and in vivo, Neurogastroenterol. Motil. 30 (2018) e13178, https://doi.org/10.1111/nmo.13178.
[7] B.H. Min, S. Devi, G.H. Kwon, H. Gupta, J.J. Jeong, S.P. Sharma, et al., Gut microbiota-derived indole compounds attenuate metabolic dysfunction-associated steatotic liver disease by improving fat metabolism and inflammation, Gut Microbes 16 (2024) 2307568, https://doi.org/10.1080/19490976.2024.2307568.
[8] B. Niu, T. Pan, Y. Xiao, H. Wang, J. Zhu, F. Tian, et al., The therapeutic potential of dietary intervention: based on the mechanism of a tryptophan derivative-indole propionic acid on metabolic disorders, Crit. Rev. Food Sci. Nutr. 8 (2024) 1–20, https://doi.org/10.1080/10408398.2023.2299744.
[9] L. Montefusco, F. D'Addio, C. Loretelli, M. Ben Nasr, M. Garziano, A. Rossi, et al., Anti-inflammatory effects of diet and caloric restriction in metabolic syndrome, J. Endocrinol. Invest 44 (2021) 2407–2415, https://doi.org/10.1007/s40618-021-01547-y.
[10] C.Y. Sun, C.J. Lin, H.C. Pan, C.C. Lee, S.C. Lu, Y.T. Hsieh, et al., Clinical association between the metabolite of healthy gut microbiota, 3-indolepropionic acid and chronic kidney disease, Clin. Nutr. 38 (2019) 2945–2948, https://doi.org/10.1016/j.clnu.2018.11.029.
[11] D.M. Lee, K.E. Ecton, S.R.J. Trikha, S.D. Wrigley, K.N. Thomas, M.L. Battson, et al., Microbial metabolite indole-3-propionic acid supplementation does not protect mice from the cardiometabolic consequences of a Western diet, Am. J. Physiol. Gastrointest. Liver Physiol. 319 (2020) G51–G62, https://doi.org/10.1152/ajpgi.00375.2019.
[12] H. Xue, X. Chen, C. Yu, Y. Deng, Y. Zhang, S. Chen, X, et al., Gut microbially produced indole-3-propionic acid inhibits atherosclerosis by promoting reverse cholesterol transport and its deficiency is causally related to atherosclerotic

cardiovascular disease, Circ. Res 131 (2022) 404–420, https://doi.org/10.1161/CIRCRESAHA.122.321253.
[13] Y.C. Wang, Y.C. Koay, C. Pan, Z. Zhou, W. Tang, J. Wilcox, et al., Indole-3-propionic acid protects against heart failure with preserved ejection fraction, Circ. Res 134 (2024) 371–389, https://doi.org/10.1161/CIRCRESAHA.123.322381.
[14] T. Kretzschmar, J. Westphal, S. Neugebauer, J.M.F. Wu, M. Zeller, J. Bogoviku, et al., Metabolic profiling identifies 1-MetHis and 3-IPA as potential diagnostic biomarkers for patients with acute and chronic heart failure with reduced ejection fraction, Circ. Heart Fail 17 (2024) e010813, https://doi.org/10.1161/CIRCHEARTFAILURE.123.010813.
[15] M. Gesper, A.B.H. Nonnast, N. Kumowski, R. Stoehr, K. Schuett, N. Marx, et al., Gut-Derived metabolite Indole-3-propionic acid modulates mitochondrial function in cardiomyocytes and alters cardiac function, Front Med (Lausanne) 8 (2021) 648259.
[16] P. Konopelski, D. Chabowski, M. Aleksandrowicz, E. Kozniewska, P. Podsadni, A. Szczepanska, et al., Indole-3-propionic acid, a tryptophan-derived bacterial metabolite, increases blood pressure via cardiac and vascular mechanisms in rats, Am. J. Physiol. Regul. Integr. Comp. Physiol. 321 (2021) R969–R981, https://doi.org/10.1152/ajpregu.00142.2021.
[17] E. Serger, L. Luengo-Gutierrez, J.S. Chadwick, G. Kong, L. Zhou, G. Crawford, et al., The gut metabolite indole-3 propionate promotes nerve regeneration and repair, Nature 607 (2022) 585–592, https://doi.org/10.1038/s41586-022-04884-x.
[18] V.D. de Mello, J. Paananen, J. Lindström, M.A. Lankinen, L. Shi, J. Kuusisto, et al., Indolepropionic acid and novel lipid metabolites are associated with a lower risk of type 2 diabetes in the Finnish Diabetes Prevention Study, Sci. Rep. 7 (2017) 46337, https://doi.org/10.1038/srep46337.
[19] M. Tuomainen, J. Lindström, M. Lehtonen, S. Auriola, J. Pihlajamäki, M. Peltonen, et al., Associations of serum indolepropionic acid, a gut microbiota metabolite, with type 2 diabetes and low-grade inflammation in high-risk individuals, Nutr. Diabetes 8 (2018) 35, https://doi.org/10.1038/s41387-018-0046-9.
[20] C. Menni, M.M. Hernandez, M. Vital, R.P. Mohney, T.D. Spector, A.M. Valdes, Circulating levels of the anti-oxidant indoleproprionic acid are associated with higher gut microbiome diversity, Gut Microbes 10 (2019) 688–695, https://doi.org/10.1080/19490976.2019.1586038.
[21] M. Pietzner, I.D. Stewart, J. Raffler, K.T. Khaw, G.A. Michelotti, G. Kastenmüller, et al., Plasma metabolites to profile pathways in noncommunicable disease multimorbidity, Nat. Med 27 (2021) 471–479, https://doi.org/10.1038/s41591-021-01266-0.
[22] Q. Qi, J. Li, B. Yu, J.Y. Moon, J.C. Chai, J. Merino, et al., Host and gut microbial tryptophan metabolism and type 2 diabetes: an integrative analysis of host genetics, diet, gut microbiome and circulating metabolites in cohort studies, Gut 71 (2022) 1095–1105, https://doi.org/10.1136/gutjnl-2021-324053.
[23] B.A. Kappel, L. De Angelis, M. Heiser, M. Ballanti, R. Stoehr, C. Goettsch, et al., Cross-omics analysis revealed gut microbiome-related metabolic pathways underlying atherosclerosis development after antibiotics treatment, Mol. Metab. 36 (2020) 100976, https://doi.org/10.1016/j.molmet.2020.100976.
[24] J. Lluch, F. Servant, S. Païssé, C. Valle, S. Valière, C. Kuchly, et al., The characterization of novel tissue microbiota using an optimized 16S metagenomic sequencing pipeline, PLoS ONE 10 (2015) e0142334, https://doi.org/10.1371/journal.pone.0142334.
[25] S. Païssé, C. Valle, F. Servant, M. Courtney, R. Burcelin, J. Amar, et al., Comprehensive description of blood microbiome from healthy donors assessed by 16S targeted metagenomic sequencing, Transfusion 56 (2016) 1138–1147, https://doi.org/10.1111/trf.13477.
[26] B.J. Callaha, A.M. Caraballo-Rodríguez, J. Chase, E.K. Cope, R. Da Silva, C. Diener, et al., Reproducible, interactive, scalable and extensible microbiome data science using QIIME 2, Nat. Biotechnol. 37 (2019) 852–857, https://doi.org/10.1038/s41587-019-0209-9.
[27] F. Pedregosa, G. Varoquaux, A. Gramfort, V. Michel, T. Bertrand, O. Grisel, et al., Scikit-learn: machine learning in python, J. Mach. Learn. Res. 12 (2011) 2825–2830.
[28] C. Quast, E. Pruesse, P. Yilmaz, J. Gerken, T. Schweer, P. Yarza, J. Peplies J, et al., The SILVA ribosomal RNA gene database project: improved data processing and web-based tools, Nucleic Acids Res 41 (2013) D590–D596, https://doi.org/10.1093/nar/gks1219.
[29] J. Chong, P. Liu, G. Zhou, J. Xia, Using microbiomeanalyst for comprehensive statistical, functional, and meta-analysis of microbiome data, Nat. Protoc. 15 (3) (2020) 799–821, https://doi.org/10.1038/s41596-019-0264-1.
[30] P.J. McMurdie, S. Holmes, phyloseq: an R package for reproducible interactive analysis and graphics of microbiome census data, PLoS One 8 (2013) e61217, https://doi.org/10.1371/journal.pone.0061217.
[31] M.E. Ritchie, B. Phipson, D. Wu, Y. Hu, C.W. Law, W. Shi, et al., limma powers differential expression analyses for RNA-sequencing and microarray studies, Nucleic Acids Res. 43 (2015) e47, https://doi.org/10.1093/nar/gkv007.
[32] P. Langfelder, S. Horvath, WGCNA: an R package for weighted correlation network analysis, BMC Bioinforma. 9 (2008) 559, https://doi.org/10.1186/1471-2105-9-559.
[33] Z.S.L. Foster, T.J. Sharpton, N.J. Grünwald, Metacoder: an R package for visualization and manipulation of community taxonomic diversity data, PLoS Comput. Biol. 13 (2017) 1–15, https://doi.org/10.1371/journal.pcbi.1005404.
[34] M.I. Love, W. Huber, S. Anders, Moderated estimation of fold change and dispersion for RNA-seq data with DESeq2, Genome Biol. 15 (2014) 550, https://doi.org/10.1186/s13059-014-0550-8.
[35] G.M. Douglas, V.J. Maffei, J.R. Zaneveld, S.N. Yurgel, J.R. Brown, C.M. Taylor, et al., PICRUSt2 for prediction of metagenome functions, Nat. Biotechnol. 38 (2020) 685–688, https://doi.org/10.1038/s41587-020-0548-6.
[36] N. Segata, J. Izard, L. Waldron, D. Gevers, L. Miropolsky, W.S. Garrett, et al., Metagenomic biomarker discovery and explanation, Genome Biol. 12 (2011) R60, https://doi.org/10.1186/gb-2011-12-6-r60.
[37] M. Venkatesh, S. Mukherjee, H. Wang, H. Li, K. Sun, A.P. Benechet, et al., Symbiotic bacterial metabolites regulate gastrointestinal barrier function via the xenobiotic sensor PXR and Toll-like receptor 4, Immunity 41 (2014) 296–310, https://doi.org/10.1016/j.immuni.2014.06.014.
[38] R. Menghini, S. Menini, R. Amoruso, L. Fiorentino, V. Casagrande, V. Marzano, et al., Tissue inhibitor of metalloproteinase 3 deficiency causes hepatic steatosis and adipose tissue inflammation in mice, Gastroenterology 136 (2009) 663–672, https://doi.org/10.1053/j.gastro.2008.10.079.
[39] C. Attané, C. Foussal, S. Le Gonidec, A. Benani, D. Daviaud, E. Wanecq, et al, Apelin treatment increases complete Fatty Acid oxidation, mitochondrial oxidative capacity, and biogenesis in muscle of insulin-resistant mice, Diabetes, 61 (2) 310-320. https://doi.org/10.2337/db11-0100.
[40] V. Casagrande, S. Menini, C. Internò, G. Pugliese, M. Federici, R. Menghini, TIMP3 overexpression in myeloid lineage alleviates pancreatic damage and confers resistance to the development of type 1 diabetes in the MLDS -induced model, Front. Endocrinol. (Lausanne) 14 (2024) 1297847, https://doi.org/10.3389/fendo.2023.1297847.
[41] C. Niaudet, B. Jung, A. Kuo, S. Swendeman, E. Bull, T. Seno, et al., Therapeutic activation of endothelial sphingosine-1-phosphate receptor 1 by chaperone-bound S1P suppresses proliferative retinal neovascularization, EMBO Mol. Med 15 (2023) e16645, https://doi.org/10.15252/emmm.202216645.
[42] M. Kurano, K. Tsukamoto, T. Shimizu, M. Hara, Y. Yatomi, Apolipoprotein M/sphingosine 1-phosphate protects against diabetic nephropathy, Transl. Res. 258 (2023) 16–34, https://doi.org/10.1016/j.trsl.2023.02.004.
[43] K. Kajit, I. Ishii, I. Mori, M. Asano, M. Fuwa, H. Morita, Sphingosine 1-phosphate regulates obesity and glucose homeostasis, Int. J. Mol. Sci. 25 (2024) 932, https://doi.org/10.3390/ijms25020932.
[44] D.K. Tobias, P.R. Lawler, P.H. Harada, O.V. Demler, P.M, J.E. Manson, et al., Circulating branched-chain amino acids and incident cardiovascular disease in a prospective cohort of US Women, Circ. Genom. Precis Med 11 (2018) e002157, https://doi.org/10.1161/CIRCGEN.118.002157.
[45] A.V. Ahola-Olli, L. Mustelin, M. Kalimeri, J. Kettunen, J. Jokelainen, J. Auvinen, et al., Circulating metabolites and the risk of type 2 diabetes: a prospective study of 11,896 young adults from four Finnish cohorts, Diabetologia 62 (2019) 2298–2309, https://doi.org/10.1007/s00125-019-05001-w.
[46] S. Christakos, S. Li, J. De La Cruz, D.D. Bikle, New developments in our understanding of vitamin metabolism, action and treatment, Metabolism 98 (2019) 112–120, https://doi.org/10.1016/j.metabol.2019.06.010.
[47] D. Yu, N.E. Richardson, C.L. Green, A.B. Spicer, M.E. Murphy, V. Flores, et al., The adverse metabolic effects of branched-chain amino acids are mediated by isoleucine and valine, Cell Metab. 33 (2021) 905–922, https://doi.org/10.1016/j.cmet.2021.03.025.
[48] H. Yin, F. Yuan, F. Jiao, Y. Niu, X. Jiang, J. Deng, et al., Intermittent leucine deprivation produces long-lasting improvement in insulin sensitivity by increasing hepatic Gcn2 expression, Diabetes 71 (2022) 206–218, https://doi.org/10.2337/db21-0336.
[49] D. Dodd, M.H. Spitzer, W. Van Treuren, B.D. Merrill, A.J. Hryckowian, S. K. Higginbottom, et al., A gut bacterial pathway metabolizes aromatic amino acids into nine circulating metabolites, Nature 551 (2017) 648–652, https://doi.org/10.1038/nature24661.
[50] Z. Chen, D. Radjabzadeh, L. Chen, A. Kurilshikov, M. Kavousi, F. Ahmadizar, Association of insulin resistance and type 2 diabetes with gut microbial diversity: a microbiome-wide analysis from population studies, JAMA Netw. Open 4 (2021) e2118811, https://doi.org/10.1001/jamanetworkopen.2021.18811.
[51] L.E. Olofsson, F. Bäckhed, The metabolic role and therapeutic potential of the microbiome, Endocr. Rev. 43 (2022) 907–926, https://doi.org/10.1210/endrev/bnac004.
[52] L. Hoyles, J.M. Fernández-Real, M. Federici, M. Serino, J. Abbott, J. Charpentier, et al., Molecular phenomics and metagenomics of hepatic steatosis in non-diabetic obese women, Nat. Med 24 (2018) 1070–1080, https://doi.org/10.1038/s41591-018-0061-3.
[53] A.M. Martin, E.W. Sun, G.B. Rogers, D.J. Keating, The influence of the gut microbiome on host metabolism through the regulation of gut hormone release, Front. Physiol. 10 (2019) 428, https://doi.org/10.3389/fphys.2019.00428.
[54] A.B. Jensen, T.I. Sørensen, O. Pedersen, T. Jess, S. Brunak, K.H. Allin, Increase in clinically recorded type 2 diabetes after colectomy, Elife 7 (2018) e37420, https://doi.org/10.7554/eLife.37420.
[55] F. D'Addio, S. La Rosa, A. Maestroni, P. Jung, E. Orsenigo, M. Ben Nasr, et al., Circulating IGF-I and IGFBP3 levels control human colonic stem cell function and are disrupted in diabetic enteropathy, Cell Stem Cell 17 (2015) 486–498, https://doi.org/10.1016/j.stem.2015.07.010.
[56] F. D'Addio, P. Fiorina, Type 1 diabetes and dysfunctional intestinal homeostasis, Trends Endocrinol. Metab. 27 (2016) 493–503, https://doi.org/10.1016/j.tem.2016.04.005.
[57] M. Karbownik, R.J. Reiter, J.J. Garcia, J. Cabrera, S. Burkhardt, C. Osuna, et al., Indole-3-propionic acid, a melatonin-related molecule, protects hepatic microsomal membranes from iron-induced oxidative damage: relevance to cancer reduction, J. Cell Biochem. 81 (2001) 507–513, https://doi.org/10.1002/1097-4644(20010601)81:3<507::aid-jcb1064>3.0.co;2-m.
[58] P. Fiorina, G. Lattuada, O. Ponari, C. Silvestrini, P. DallAglio, Impaired nocturnal melatonin excretion and changes of immunological status in ischaemic stroke patients, Lancet 347 (1996) 692–693, https://doi.org/10.1016/S0140-6736(96)91246-5.

[59] Y.J. Chyan, B. Poeggeler, R.A. Omar, D.G. Chain, B. Frangione, J. Ghiso, et al., Potent neuroprotective properties against the Alzheimer beta-amyloid by an endogenous melatonin-related indole structure, indole-3-propionic acid, J. Biol. Chem. 274 (1999) 21937–21942, https://doi.org/10.1074/jbc.274.31.21937.
[60] B.H. Min, S. Devi, G.H. Kwon, H. Gupta, J.J. Jeong, S.P. Sharma, et al., Gut microbiota-derived indole compounds attenuate metabolic dysfunction-associated steatotic liver disease by improving fat metabolism and inflammation, Gut Microbes 16 (2024) 2307568, https://doi.org/10.1080/19490976.2024.2307568.
[61] M. Gesper, A.B.H. Nonnast, N. Kumowski, R. Stoehr, K. Schuett, N. Marx, B.A, et al., Gut-derived metabolite indole-3-propionic acid modulates mitochondrial function in cardiomyocytes and alters cardiac function, Front. Med. (Lausanne) 8 (2021) 648259, https://doi.org/10.3389/fmed.2021.648259.
[62] C.T. Capaldo, Claudin barriers on the brink: how conflicting tissue and cellular priorities drive IBD pathogenesis, Int. J. Mol. Sci. 24 (2023) 8562, https://doi.org/10.3390/ijms24108562.
[63] Z. Chen, J. Luo, J. Li, G. Kim, E.S. Chen, S. Xiao, et al., Foxo1 controls gut homeostasis and commensalism by regulating mucus secretion, J. Exp. Med. 218 (2021) e20210324, https://doi.org/10.1084/jem.20210324.